Image-based computational model for focused ultrasound ablation of liver tumor

Maxim A Solovchuk[1*], Tony WH Sheu[1,2*] and Marc Thiriet[3]

*Correspondence:
solovchuk@gmail.com;
twhsheu@ntu.edu.tw
[1]Center of Advanced Study in
Theoretical Sciences (CASTS),
National Taiwan University,Taipei,
Taiwan
[2]Department of Engineering
Science and Ocean Engineering,
National Taiwan University,No. 1,
Sec. 4, Roosevelt Road, Taipei
Full list of author information is
available at the end of the article

Abstract

High-intensity focused ultrasound (HIFU) is a rapidly developing medical technology that allows non-invasive thermal ablation of tumors. Thermal treatment of liver tumor, which is one of the most common malignancies worldwide, is problematic because large blood vessels act as a heat sink. Convective cooling protects the cancer cells from thermal destruction and decreases the necrosed volume. A major objective of the method development is to achieve a virtually complete necrosis of tumors close to major blood vessels and to avoid blood vessel damage and, hence, the needed treatment planning. The present study is aimed at predicting liver tumor temperature during HIFU thermal ablation in a patient-specific liver geometry. The model comprises the nonlinear Westervelt equation and bioheat equations in the liver and blood vessels. The nonlinear hemodynamic equations are also taken into account with the convected cooling and acoustic streaming effects being taken into account. We found from this three-dimensional three-field coupling study that in large blood vessels, both convective cooling and acoustic streaming may change the temperature considerably near the blood vessel. More precisely, acoustic streaming velocity magnitude can be several times larger than the blood vessel velocity. The results presented in the current work can be further used to construct a surgical planning platform.

Keywords: HIFU; Liver tumor; Blood vessel; Westervelt equation; Acoustic streaming.

Background

High-intensity focused ultrasound (HIFU) is a therapeutic method for a non-invasive ablation of benign and malignant tumors [1,2]. The main mechanism of tissue ablation is thermal coagulation. Temperature about 60°C can cause an irreversible tissue damage. Liver cancer is the second leading cause of death in Asia [3] and is now known as one of the leading causes of death in the world. The primary problem in the thermal ablation therapy of liver tumor is due to a heat sink resulting from the blood flow in large blood vessels.

Convective cooling protects tumor cells from thermal destruction [4,5] and, consequently, causes the recurrent cancer. Blood flow can carry away a large part of the deposited energy; therefore, more energy is necessary for the ablation of tumor close to blood vessel. This can lead to the use of redundant ultrasound powers and undesirable damage of healthy tissues. Special care should be taken to avoid destruction of vessel walls by a high temperature. In some studies it was reported that high-intensity focused ultrasound can cause occlusion of blood vessels and blood vessel disruption [6,7]. A basic

understanding of the factors that can altogether influence the tissue necrosis volume is necessary to improve the thermoablative therapy and prevent recurrence.

One clinical trial in [8] showed that HIFU can safely necrotize the tumors close to major hepatic veins. Before HIFU treatment, some patients had transcatheter chemoemboliza- tion. After a single session of HIFU treatment, the rate of complete necrosis was about 50%, which is not satisfactory at all. Lack of a complete response can be attributed to the large tumor size and the cooling effect in large vessels.

Liver is a highly perfused organ with a blood supply from the hepatic artery and portal vein. In most of the previous computational studies, liver is considered as a homogeneous tissue, and the amount of dissipated heat is usually estimated by averaging the effect of blood perfusion over all tissues [9]. This approach is valid for tissues with capillaries. However, for tissues with thermally significant blood vessels (diameters larger than 0.5 mm) the biologically relevant convective cooling needs to be taken into account [10], and homogenization assumption is no longer valid. Kolios et al. [10] and Curra et al. [11] studied the influence of blood vessels on the lesion size based on a 2D finite difference calculation in the cylindrical coordinate system. The focal point was at the center of the blood vessel. In this case, a large portion of the deposited ultrasound energy was carried away by convective cooling. Recently, a three-dimensional (3D) model to determine the influence of blood flow on the temperature distribution was presented [12,13]. To get the velocity distribution for a real blood vessel geometry, nonlinear hemodynamic equations were used. Focused ultrasound beam can induce an additional mass flow in blood ves- sels. This effect is known as an acoustic streaming. Acoustic streaming can increase the velocity magnitude in a blood vessel, strengthen the heat sink, and change the temper- ature distribution near the blood vessel [13]. Therefore, the effect of acoustic streaming was taken into account in the present study.

In the present work, temperature elevation in the liver tumor is considered in a patient- specific geometry. Tumor is located close to the portal vein with the diameter about 7 mm. The theoretical feasibility to ablate tumor close to the portal vein was shown. The results presented in the current work can be further used to construct a surgical plan- ning platform. The computational model can play an important role in the planning and optimization of the treatment based on the patient's image.

Methods

Nonlinear acoustic equation

Acoustic field generated by a HIFU source was modeled using the nonlinear Westervelt equation [14]:

$$\nabla^2 p - \frac{1}{c_0^2}\frac{\partial^2 p}{\partial t^2} + \frac{\delta}{c_0^4}\frac{\partial^3 p}{\partial t^3} + \frac{\beta}{\rho_0 c_0^4}\frac{\partial^2 p^2}{\partial t^2} = 0 \tag{1}$$

In the above, p is the sound pressure, $\beta = 1 + \frac{B}{2A}$ the coefficient of nonlinearity, and δ the diffusivity of sound. The first two terms describe the linear lossless wave propagating at a small-signal sound speed. The third term represents the loss due to thermal con- duction and fluid viscosity. The last term accounts for acoustic nonlinearity which may considerably affect thermal and mechanical changes within the tissue.

In soft tissues, acoustic diffusivity accounts for the thermal and viscous losses in a fluid and it is modeled by

$$\delta = \frac{2c_0^3 \alpha_{\mathrm{abs}}}{\omega^2},\tag{2}$$

where α_{abs} denotes the acoustic absorption coefficient.

The ultrasound power deposition per unit volume can be calculated as follows [15,16]:

$$q = \frac{2\alpha_{\mathrm{ABS}}}{\rho_0 c_0 \omega^2} < \left(\frac{\partial p}{\partial t}\right)^2 > = \frac{2\alpha_{\mathrm{ABS}}}{\rho_0 c_0 \omega^2} \frac{1}{T} \int\limits_0^T \left(\frac{\partial p}{\partial t}\right)^2 dt\tag{3}$$

Energy equation for tissue heating

Whereas hepatic arteries and portal veins irrigate the liver parenchyma, hepatic veins drain blood out of the liver and can thus be considered as a heat sink. Tumor cells in perivascular region, as a result, may escape from an externally imposed large heat, leading possibly to a local recurrence. Therefore, the mathematical model suitable for predicting the temperature in tissues must take the heat conduction, tissue perfusion, convective blood cooling, and heat deposition due to an incident wave into account. In the simulation of the thermal field, the physical domain has been split into the domains for the perfused tissue and the flowing blood.

In a region free of large blood vessels, the diffusion-type Pennes bioheat equation [9] given below is employed to model the transfer of heat in the perfused tissue region

$$\rho_t \, c_t \frac{\partial T}{\partial t} = k_t \nabla^2 T - w_b \, c_b \, (T - T_\infty) + q\tag{4}$$

In the above bioheat equation proposed for modeling the time-varying temperature in tissue domain, ρ, c, and k denote the density, specific heat, and thermal conductivity, respectively, with the subscripts t and b referring to the tissue and blood domains, respectively. The notation T_∞ is denoted as the temperature at a remote location. The variable w_b ($\equiv 10$ kg/m^3 s) in Equation 4 is the perfusion rate for the tissue cooling in capillary flows. It is noted that the above bioheat equation for T is coupled with the Westervelt equation (1) for the acoustic pressure through a power deposition term q defined in Equation 3.

In the region containing large vessels, within which the blood flow can convect heat, the biologically relevant heat source, which is q, and the heat sink, which is $-\rho_b \, c_b \, \underline{\mathbf{u}} \cdot \nabla T$, are added to the conventional diffusion-type heat equation. The resulting energy equation given below avoids a possible high recurrence stemming from the tumor cell survival next to large vessels

$$\rho_b \, c_b \frac{\partial T}{\partial t} = k_b \nabla^2 T - \rho_b \, c_b \, \underline{\mathbf{u}} \cdot \nabla T + q\tag{5}$$

In the above equation, $\underline{\mathbf{u}}$ is the blood flow velocity. Owing to the presence of blood flow velocity vector $\underline{\mathbf{u}}$ in the energy equation, a biologically sound model needed for conducting a HIFU simulation should comprise a coupled system of thermal-fluid-acoustics nonlinear differential equations.

Thermal dose developed by Sapareto and Dewey [17] will be applied to give us a quantitative relationship between the temperature and time for the tissue heating and the extent

of cell killing. In focused ultrasound surgery (generally above 50°C), the expression for the thermal dose (TD) can be written as

$$\text{TD} = \int_{t_0}^{t_{\text{final}}} R^{(T-43)} dt \approx \sum_{t_0}^{t_{\text{final}}} R^{(T-43)} \Delta t, \tag{6}$$

where $R = 2$ for $T >= 43$°C, $R = 4$ for 37°C $< T < 43$°C. The value of TD required for a total necrosis ranges from 25 to 240 min in biological tissues [13,17,18]. According to this relation, thermal dose resulting from heating the tissue to 43°C for 240 min is equivalent to that achieved by heating it to 56°C for 1 s.

Acoustic streaming hydrodynamic equations

Owing to the inclusion of the heat sink, which is shown on the right-hand side of Equation 5, the velocity of blood flow plus the velocity resulting from the acoustic streaming due to the applied high-intensity ultrasound must be determined. In this study, we consider that the flow in the large blood vessels is incompressible and laminar. The vector equation for modeling blood flow motion, subject to the divergence-free equation $\nabla \cdot \underline{\mathbf{u}} = 0$, in the presence of acoustic stresses is as follows [19]:

$$\frac{\partial \underline{\mathbf{u}}}{\partial t} + (\underline{\mathbf{u}} \cdot \nabla)\underline{\mathbf{u}} = \frac{\mu}{\rho}\nabla^2\underline{\mathbf{u}} - \frac{1}{\rho}\nabla\mathbf{P} + \frac{1}{\rho}\underline{\mathbf{F}} \tag{7}$$

In the above equation, $\mathbf{P}$ is the static pressure, μ ($= 0.0035$ kg/m s) the shear viscosity of blood flow, and ρ the blood density. In Equation 7, the force vector $\underline{\mathbf{F}}$ acting on the blood fluid due to ultrasound is assumed to be along the acoustic axis $\underline{\mathbf{n}}$. The resulting nonzero component in $\underline{\mathbf{F}}$ takes the following form [20]:

$$\underline{\mathbf{F}} \cdot \underline{\mathbf{n}} = \frac{2\alpha_{\text{ABS}}}{\rho_0 c_0^2 \omega^2} < \left(\frac{\partial p}{\partial t}\right)^2 > \tag{8}$$

Three-point sixth-order accurate scheme for Westervelt equation

Discretization of the Westervelt equation (1) is started with the temporal derivatives. Temporal derivatives were calculated by the second-order accurate schemes given as follows:

$$\left.\frac{\partial^2 p}{\partial t^2}\right|^{n+1} = \frac{2p^{n+1} - 5p^n + 4p^{n-1} - p^{n-2}}{(\Delta t)^2} \tag{9}$$

$$\left.\frac{\partial^3 p}{\partial t^3}\right|^{n+1} = \frac{6p^{n+1} - 23p^n + 34p^{n-1} - 24p^{n-2} + 8p^{n-3} - p^{n-4}}{2(\Delta t)^3} \tag{10}$$

The nonlinear term $\frac{\partial^2 p^2}{\partial t^2}\big|^{n+1}$ is linearized using the second-order accurate relation:

$$\begin{aligned}
\left.\frac{\partial^2 p^2}{\partial t^2}\right|^{n+1} &= \frac{\partial}{\partial t}\left(\frac{\partial p^2}{\partial t}\right)\Big|^{n+1} = 2\frac{\partial}{\partial t}\left(p^n \frac{\partial p}{\partial t}\Big|^{n+1} + p^{n+1}\frac{\partial p}{\partial t}\Big|^n - p^n\frac{\partial p}{\partial t}\Big|^n\right) \\
&= 2\left(2p_t^n p_t^{n+1} + p^n p_{tt}^{n+1} + p^{n+1}p_{tt}^n - (p_t^n)^2 - p^n p_{tt}^n\right)
\end{aligned} \tag{11}$$

The above Equations (9, 10, 11) are then substituted into Equation 1 to yield the following inhomogeneous Helmholtz equation:

$$u_{xx} - ku = f(x) \tag{12}$$

High-order Helmholtz schemes can be constructed by introducing more finite-difference stencil points. The improved prediction accuracy is, however, at the cost of an

increasingly expensive matrix calculation. To retain the prediction accuracy at a lower computational cost, we are motivated to develop a scheme that can give us the accuracy order of six in a grid stencil involving only three points. To achieve the above goal, we define firstly the spatial derivatives $u^{(2)} \equiv u_{xx}$, $u^{(4)} \equiv u_{xxxx}$ and $u^{(6)}$ at a nodal point j as follows:

$$u^{(2)}|_j = s_j, \ u^{(4)}|_j = t_j, \ u^{(6)}|_j = w_j \tag{13}$$

Development of the compact scheme at x_j is to relate t, s, and w with u as follows:

$$h^6 \delta_0 w_j + h^4 \gamma_0 t_j + h^2 \beta_0 s_j = \alpha_1 u_{j+1} + \alpha_0 u_j + \alpha_{-1} u_{j-1} \tag{14}$$

By substituting the Taylor series expansion into Equation 14 and then conducting a term-by-term comparison of the derivatives, the introduced free parameters can be determined as $\alpha_1 = \alpha_{-1} = -1$, $\alpha_0 = 2$, $\beta_0 = -1$, $\gamma_0 = -\frac{1}{12}$, and $\delta_0 = -\frac{1}{360}$.

Since $s_j = k_j u_j + f_j$, the following two expressions for $t_j = (k_j^2 u_j + 2k_{x,j} u_{x,j} + k_{xx,j} u_j + k_j f_j + f_{xx,j})$ and $w_j = (k_j^3 u_j + 7k_j u_j k_{xx,j} + 6k_j u_{x,j} k_{x,j} + 4k_{x,j}^2 u_j + 6k_{xx,j} f_j + 4k_{xxx,j} u_{x,j} + k_{xxxx,j} u_j + 4k_{x,j} f_{x,j} + k_j f_{xx,j} + f_{xxxx,j})$ are resulted. Equation 14 can then be rewritten as

$$
\begin{aligned}
& \alpha_1 u_{j+1} + \alpha_1 u_{j-1} \\
& + \left[\alpha_0 - \beta_0 \, h^2 \, k_j - \gamma_0 \, h^4 \left(k_j^2 + k_{xx,j} \right) - \delta_0 \, h^6 \left(k_j^3 + 7k_j k_{xx,j} + +4k_{x,j}^2 + k_{xxxx,j} \right) \right] u_j \\
& = h^2 \beta_0 f_j + h^4 \gamma_0 \left(2k_{x,j} u_{x,j} + k_j f_j + f_{xx,j} \right) + h^6 \delta_0 \left(k^2 f_j + k f_{xx,j} + f_{xxxx,j} \right) \\
& + h^6 \delta_0 \left(6k_j u_{x,j} k_{x,j} + 6k_{xx,j} f_j + 4k_{xxx,j} u_{x,j} + 4k_{x,j} f_{x,j} \right)
\end{aligned}
\tag{15}
$$

It follows that

$$
\begin{aligned}
& \left[1 - \left(\frac{1}{2h} - \frac{k_{j+1}h}{12} \right) \left(\frac{1}{360} h^6 (4k_{xxx,j} + 6k_j k_{x,j}) + \frac{1}{6} h^4 k_{x,j} \right) \right] u_{j+1} \\
& - \left[2 + h^2 k_j + \frac{1}{12} h^4 \left(k_j^2 + k_{xx,j} \right) + \frac{1}{360} h^6 \left(k_j^3 + 4k_{x,j}^2 + 7k_j k_{xx,j} + k_{xxxx,j} \right) \right] u_j \\
& + \left[1 + \left(\frac{1}{2h} - \frac{k_{j-1}\,h}{12} \right) \left(\frac{1}{360} \, h^6 (4\,k_{xxx,j} + 6\,k_j\,k_{x,j}) + \frac{h^4 \, k_{x,j}}{6} \right) \right] u_{j-1} \\
& = \left[h^2 + \frac{k_j h^4}{12} + \frac{1}{360} h^6 \left(k_j^2 + 6k_{xx,j} \right) \right] f_j + \frac{1}{90} h^6 k_{x,j} f_{x,j} + \left(\frac{1}{360} h^6 \, k_j + \frac{1}{12} h^4 \right) f_{xx,j} \\
& + \frac{1}{360} h^6 f_{xxxx,j} + \left[\frac{1}{6} \, h^4 k_{x,j} + \frac{1}{360} h^6 \left(6k_j k_{x,j} + 4k_{xxx,j} \right) \right] \cdot \left[-\frac{h}{12} \left(f_{j+1} - f_{j-1} \right) \right]
\end{aligned}
\tag{16}
$$

The corresponding modified equation for (12) using the currently proposed compact scheme can be derived as follows after performing some algebraic manipulation:

$$u_{xx} - ku = f + \left(\frac{h^6}{20,160} \right) u^{(8)} + \left(\frac{h^8}{1,814,400} \right) u^{(10)} + \cdots + \text{HOT}, \tag{17}$$

where HOT denotes higher order terms. The above modified equation analysis sheds light that the Helmholtz scheme developed within the three-point stencil framework can yield a spatial accuracy order of six. Axisymmetric sound beam was considered. The Westervelt equation was solved in conjunction with the alternating direction implicit solution algorithm [21]. Absorbing boundary conditions were applied to prevent numerical reflections. Accuracy of the numerical solutions was examined [22] by comparing with the known analytical and numerical solutions of other authors.

Table 1 Acoustic and thermal properties for the liver tissue and blood

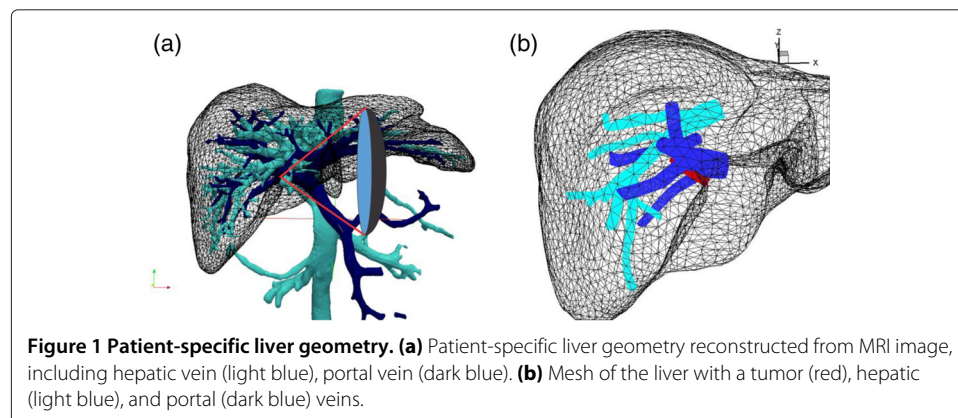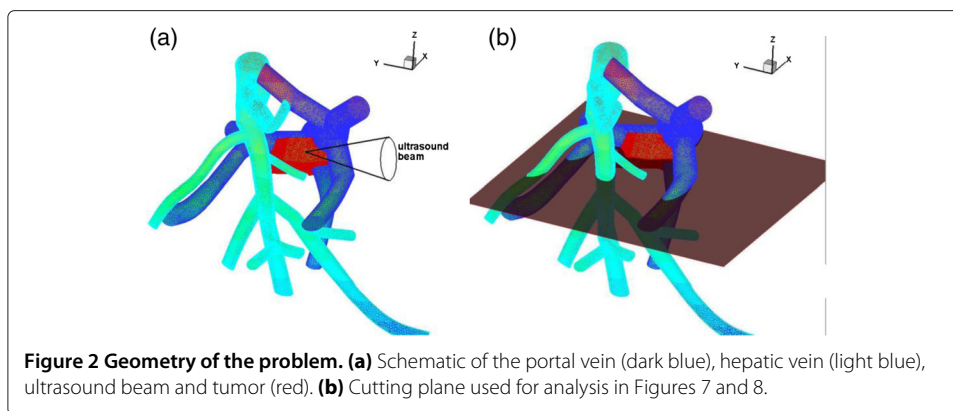| Tissue	$c_0(\frac{m}{s})$	$\rho(\frac{kg}{m^3})$	$c(\frac{J}{kgK})$	$k(\frac{W}{mK})$	$\alpha(\frac{Np}{m})$
Liver	1,540	1,055	3,600	0.512	8.1
Blood	1,540	1,060	3,770	0.53	1.5

Problem description

The single element HIFU transducer (frequency 1 MHz) used in this study is spherically focused with an aperture of 12 cm and a focal length of 12 cm. This transducer presumably emits a beam of spherically shaped ultrasound wave propagating towards the targeted tissue under the current investigation. The solid tumor was assumed to be exposed to a 1.7-s ultrasound. The parameters used in the current simulation are listed in Table 1 [23]. The three-dimensional problem is analyzed using finite-volume method. A detailed description of the solution procedures can be found in our previous articles [12,13,24]. Initially, we consider that the temperature is equal to 37°C. The blood viscosity is 0.0035 kg/(m s). A no-slip boundary condition is applied on the vessel wall.

The present numerical experiments are carried out in a patient-specific liver model. A reconstructed surface mesh for the hepatic vein, portal vein and liver is presented in Figure 1a. Simulation for the whole liver geometry requires a large amount of computer resource. To save computational time, only the portal and hepatic venous networks close to tumor in the right part of the liver are used in the simulation (Figure 2). The reconstructed mesh for the liver, solid tumor, and hepatic and portal veins is presented in Figure 1b. The total number of tetrahedral elements used in this study is 910,000. In the focal region, the refined grids were generated with a mesh length 0.2 mm.

Results and discussion

In Figure 3, the predicted linear and nonlinear pressures along the beam axis y (a) and pressure waveforms at the focal point (b) are presented. At high intensities, nonlinear wave propagation effects lead to the distortion of waveform. Due to the nonlinear distortion, higher harmonics are generated. These higher harmonics are more readily absorbed by the tissue, enhancing therefore local heating. The peak positive and negative pressures are $P_+ = 7.7$ MPa and $P_- = 5.3$ MPa, respectively. The linear theory predicts focal pressure $P_L = 6.2$ MPa. The peak power deposition increased 17% from the linear to nonlinear waveform. The solid tumor was assumed to be exposed to a 1.7-s ultrasound.

Figure 1 Patient-specific liver geometry. (a) Patient-specific liver geometry reconstructed from MRI image, including hepatic vein (light blue), portal vein (dark blue). **(b)** Mesh of the liver with a tumor (red), hepatic (light blue), and portal (dark blue) veins.

Figure 2 Geometry of the problem. (a) Schematic of the portal vein (dark blue), hepatic vein (light blue), ultrasound beam and tumor (red). **(b)** Cutting plane used for analysis in Figures 7 and 8.
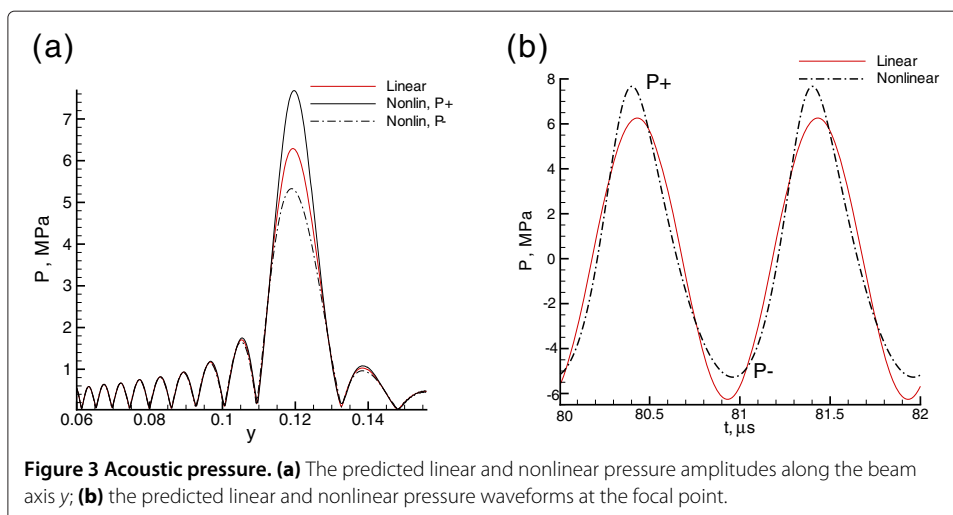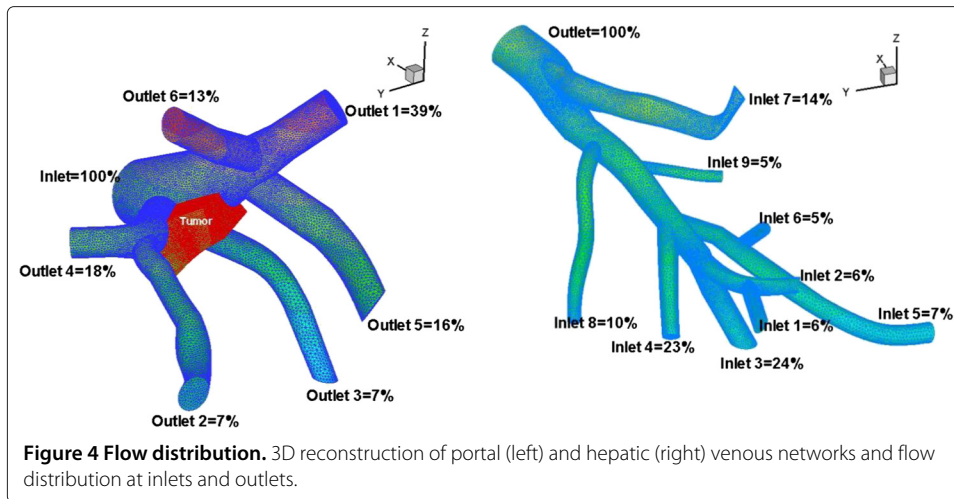
Three-dimensional reconstruction of portal and hepatic venous networks and flow distribution at inlets and outlets is presented in Figure 4. Mass balance analysis shows that the total mass flux at inlet is equal to the total mass fluxes at outlets.

Acoustic streaming is considered as a second-order physical effect in the HIFU therapy and is usually neglected. To investigate the importance of acoustic streaming effect during the thermal therapy, we have calculated hydrodynamic equation (Equation 7) with and without acoustic source given in (8). Velocity profiles at different cutting planes in portal and hepatic venous network are presented in Figures 5, 6, and 7 with and without acoustic streaming effect. Maximum velocity magnitudes in the portal vein for the cases considered with and without acoustic streaming are 0.26 and 0.09 m/s, respectively. Acoustic streaming increases the velocity magnitude by three times. This will increase the blood flow cooling and decrease the temperature rise. For the hepatic vein (Figure 6), the difference in velocity for the cases considered with and without acoustic streaming is negligibly small because hepatic vein is located far from the focal point and the acoustic axis of ultrasound beam.
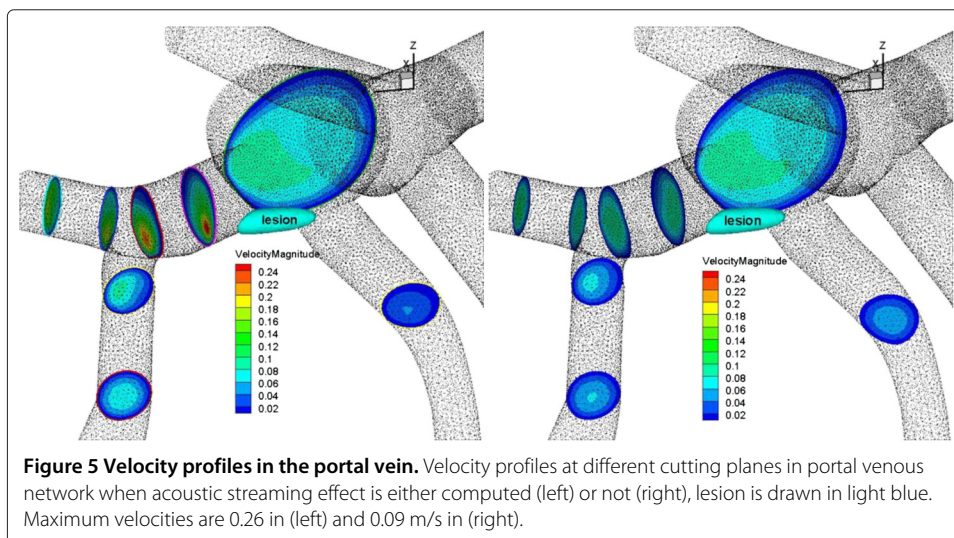
The simulated temperature contours in the tumor and in the portal vein at the cutting plane $z = 0.16$ are presented in Figure 8 at time $t = 1.7\,s$ (end of sonication). Calculation shows that tumor close to the blood vessel can be ablated. There is a very sharp

Figure 3 Acoustic pressure. (a) The predicted linear and nonlinear pressure amplitudes along the beam axis *y*; **(b)** the predicted linear and nonlinear pressure waveforms at the focal point.

Figure 4 Flow distribution. 3D reconstruction of portal (left) and hepatic (right) venous networks and flow distribution at inlets and outlets.
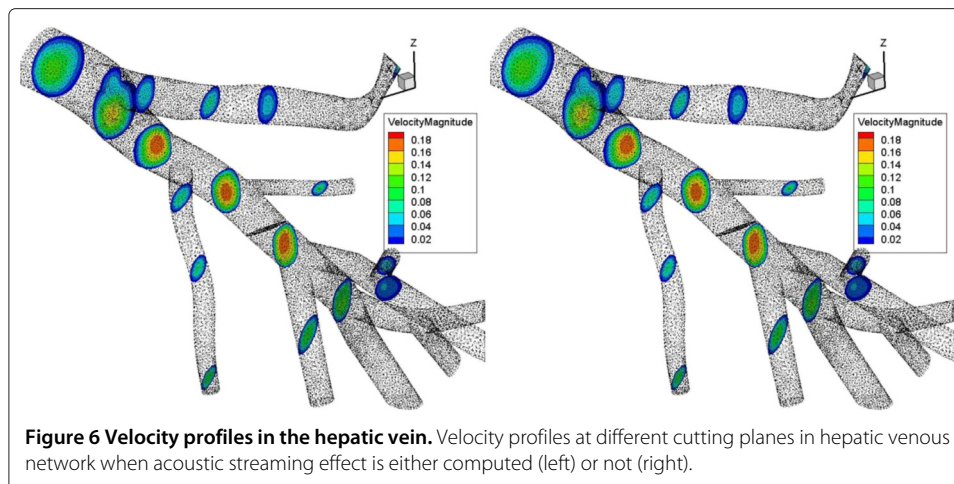
temperature gradient near the blood vessel wall. We can see a strong asymmetry in the lesion shape due to blood flow cooling. The temperature inside the blood vessel remains almost unchanged except the boundary layer close to the focal point. Therefore, focused ultrasound can be a safe therapy to ablate tumors close to the blood vessel wall. However, additional experimental studies *in vitro* and *in vivo* are necessary [8]. Simulation results can help to optimize an appropriate sonication time, ultrasound power and focal point location.

In Table 2, we present the predicted mass fluxes at the inlet and six outlets in the portal vein with and without acoustic streaming. We can see that mass fluxes at outlets can be redistributed and the acoustic streaming effect cannot be ignored because it can cause a considerable redistribution of the mass flux, up to 46% difference in our case at outlet 4. There is an increase of mass fluxes at outlets 2 and 4 and a decrease of mass fluxes at outlets 1, 3, 5, and 6. The largest difference in mass fluxes with and without acoustic streaming is at outlets 2 and 4 because they are located close to the tumor (Figures 4

Figure 5 Velocity profiles in the portal vein. Velocity profiles at different cutting planes in portal venous network when acoustic streaming effect is either computed (left) or not (right), lesion is drawn in light blue. Maximum velocities are 0.26 in (left) and 0.09 m/s in (right).

Figure 6 Velocity profiles in the hepatic vein. Velocity profiles at different cutting planes in hepatic venous network when acoustic streaming effect is either computed (left) or not (right).
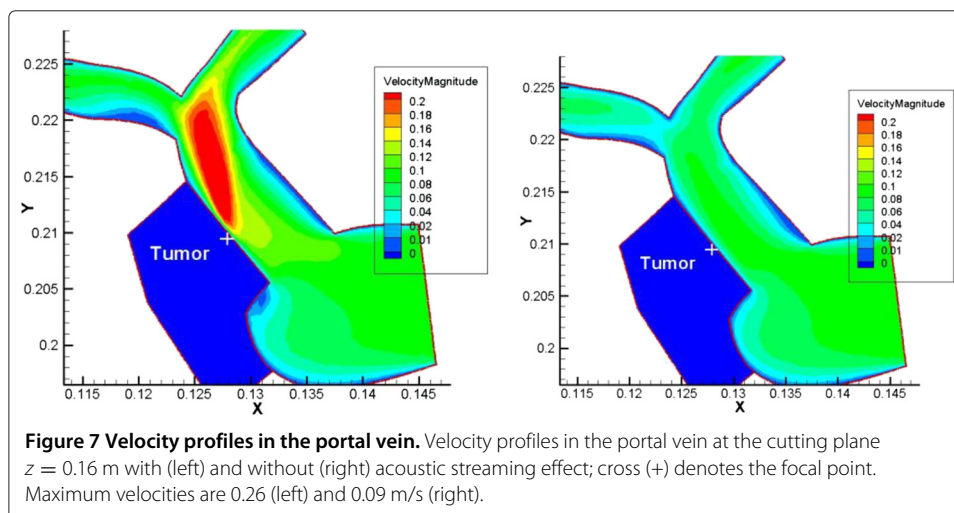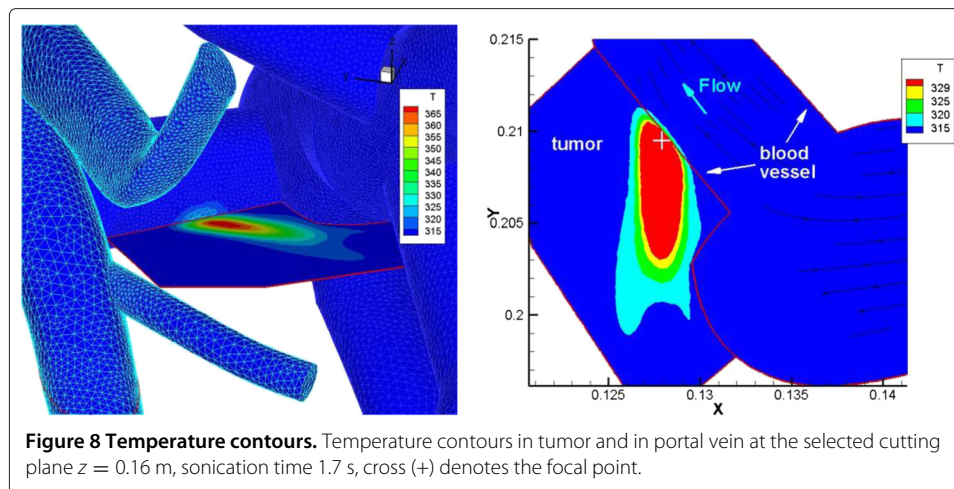
and 9). This effect can also be used to control drug delivery. In the present study, acoustic streaming leads to mass flux redistribution and increases the velocity magnitude by three times. This will increase the blood flow cooling and decrease the temperature rise. Temperature difference on the portal vein wall with and without acoustic streaming is presented in Figure 10. The maximum wall temperature difference is 4.8 K. This shows the importance of the acoustic streaming effect.

The present work demonstrates interference between the parenchymal blood flow and the heat locally transferred to the hepatic parenchyma by ultrasound. On the one hand, the temperature field is affected by blood flow cooling. On the other hand, acoustic streaming resulting from an emitted ultrasound for thermal ablation changes the flow distribution according to the location of large blood vessels with respect to that of the tumor. The closer the vessels to the tumor, the higher the increase of flow rate. Therefore, acoustic streaming contributes to blood flow cooling.

In the present work, the tumor was located close to the blood vessel with the diameter $d = 7$ mm. For smaller blood vessel diameters, the effect of acoustic streaming will be

Figure 7 Velocity profiles in the portal vein. Velocity profiles in the portal vein at the cutting plane $z = 0.16$ m with (left) and without (right) acoustic streaming effect; cross (+) denotes the focal point. Maximum velocities are 0.26 (left) and 0.09 m/s (right).

Figure 8 Temperature contours. Temperature contours in tumor and in portal vein at the selected cutting plane $z = 0.16$ m, sonication time 1.7 s, cross (+) denotes the focal point.

smaller. In [24,25], the importance of blood flow cooling and acoustic streaming was studied for parallel and perpendicular blood vessel orientations. Intermediate intensity range was considered. It was shown that when the distance between the tumor and blood vessel wall is less than several millimeters, the convective cooling should be taken into account and the homogenization assumption becomes no longer acceptable. If the blood vessel is inside the area of the beam, inside the half-pressure maximum (-6 dB) contours, the effect of acoustic streaming should be taken into account. For the case of high intensities, the effect of acoustic streaming becomes important in the larger area. For blood vessels with a smaller diameter, the effect of acoustic streaming becomes less important. It was shown that if the diameter of the blood vessel is smaller than 1 mm acoustic streaming velocity magnitude is smaller than blood flow velocity [24]. However, only intermediate intensity range was considered. For the high-intensity focused ultrasound, acoustic streaming velocity magnitude will be larger and additional parametric studies may be necessary. In the near future, it is highly interesting to investigate the threshold size of blood vessel and the distance between the tumor and blood vessel wall beyond which the acoustic streaming effects should be considered negligibly small in the modeling and calculations.
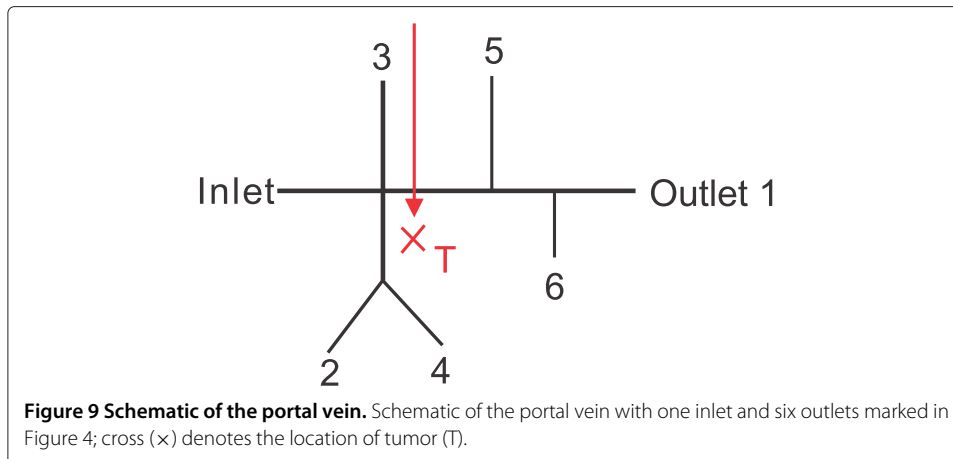
Personalized liver cancer treatment planning is necessary based on the appropriate image acquisition and processing not only to localize the tumor inside the parenchymal arterial trees and venous drainage network, but also to detect possible small additional tumors more or less close to the main tumor. The existence of these additional foci is the indication for surgical resection.

Post HIFU regrowth depends mainly on the distance between the tumor and large blood vessels. This technique is not used when the distance is too short. Under the circumstances, the surgery is the selected treatment. When the distance is long enough, but
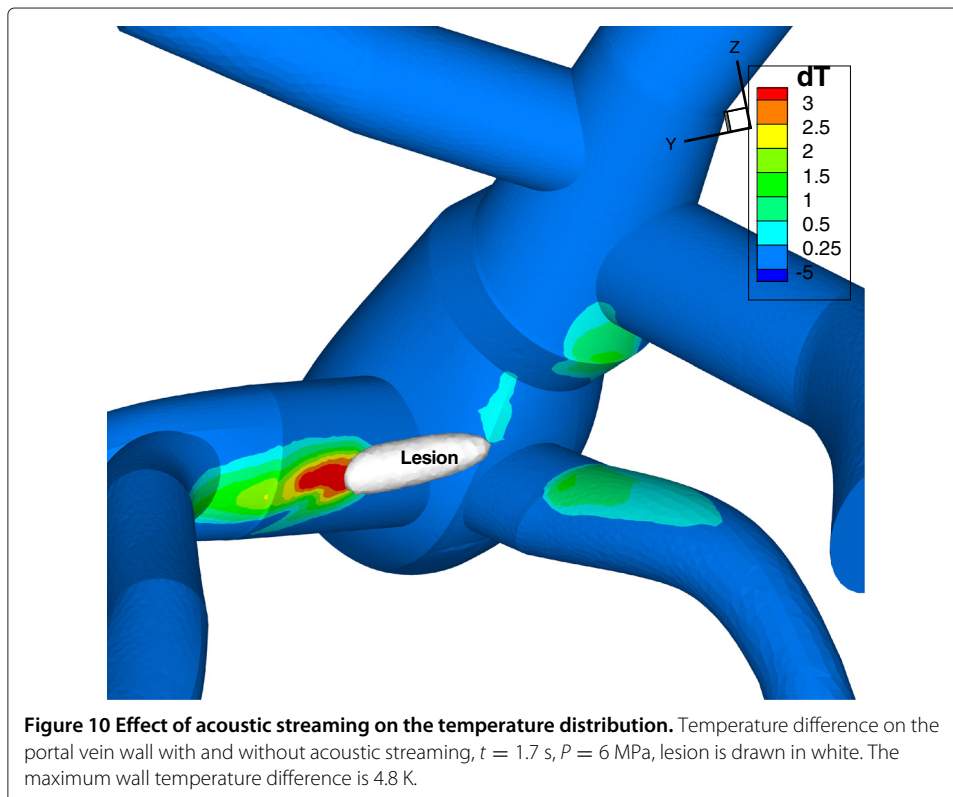
Table 2 Mass flux

	Outlet 1	Outlet 2	Outlet 3	Outlet 4	Outlet 5	Outlet 6	Inlet
Without AS	$4.08 \cdot 10^{-3}$	$7.59 \cdot 10^{-4}$	$6.96 \cdot 10^{-4}$	$1.85 \cdot 10^{-3}$	$1.615 \cdot 10^{-3}$	$1.40 \cdot 10^{-3}$	$1.04 \cdot 10^{-2}$
With AS	$3.70 \cdot 10^{-3}$	$9.80 \cdot 10^{-4}$	$5.07 \cdot 10^{-4}$	$2.7 \cdot 10^{-3}$	$1.30 \cdot 10^{-3}$	$1.22 \cdot 10^{-3}$	$1.04 \cdot 10^{-2}$
Difference	-9%	*+29.0%*	-27%	*+46%*	-20%	-13%	

Acoustic streaming (AS) effect on the mass flux in the portal vein. Mass flux (kg/s).

Figure 9 Schematic of the portal vein. Schematic of the portal vein with one inlet and six outlets marked in Figure 4; cross (×) denotes the location of tumor (T).

remains short, US intensity is limited to avoid a strong vascular damage. The destruction of cancerous cells may then be partial. The post-therapeutic control of the liver must be carefully carried out to ensure that a rapid tumor regrowth does not appear. In the case of tumor reoccurrence, surgery can then be performed. This medical strategy can be used when surgery must be delayed because of the patient state does not enable it. The proper case corresponds to a tumor at distance from large blood vessels, for which the highest admissible dose (US power and duration) can be used.

There are several ways to stop blood flow in portal veins and in hepatic veins either pharmacologically or physically. The proposed mathematical model can be used to predict temperature elevation during the treatment in this case. If blood flow was stopped, it

Figure 10 Effect of acoustic streaming on the temperature distribution. Temperature difference on the portal vein wall with and without acoustic streaming, $t = 1.7$ s, $P = 6$ MPa, lesion is drawn in white. The maximum wall temperature difference is 4.8 K.

will be easier to ablate tumor close to the blood vessel wall. However, due to a high temperature, the blood vessel wall can be damaged or the blood vessel can be occluded [7]. Prior to the treatment, the model can predict whether the blood vessel will be damaged or not. Depending on the anticipated goals, the current model can be used to optimize ultrasound power and treatment time.

The current work is a first step towards the development of HIFU treatment planning platform. This platform can be used to optimize treatment time and applied ultrasound powers in order to minimize damage of healthy tissues and to destroy all cancer cells.

Conclusion

The proposed three-dimensional physical model for HIFU study was conducted in an image-based liver geometry. Usually, during the treatment planning, effect of blood flow cooling is not taken into account. In the present work, we showed that both blood flow cooling and acoustic streaming effects can significantly affect the treatment and both of them should be taken into account. At high intensities, the effect of cooling by acoustic streaming can prevail over convective cooling in large blood vessels. The theoretical feasibility to necrotize the tumors close to major veins was shown. It was shown that tumors close to the blood vessel wall can be ablated without damaging the blood vessel wall. These results can be further used to construct a surgical planning platform for the non-invasive HIFU tumor ablating therapy in real liver geometry from MRI image and can lead in the future to the improvement of the focused ultrasound ablation of liver tumor. The presented model can be used to develop similar planning tools for other organs.

Author details
[1]Center of Advanced Study in Theoretical Sciences (CASTS), National Taiwan University,Taipei, Taiwan. [2]Department of Engineering Science and Ocean Engineering, National Taiwan University,No. 1, Sec. 4, Roosevelt Road, Taipei. [3]LJLL, University Pierre and Marie Curie,Paris, France.

References
1. Zhou Y: **High intensity focused ultrasound in clinical tumor ablation.** *World J Clin Oncol* 2011, **2:**8–27.
2. Leslie T, Kennedy J: **High intensity focused ultrasound in the treatment of abdominal and gynaecological diseases.** *Int J Hyperthermia* 2007, **23**(2):173–182.
3. Huang JS, Gervais D, Mueller P: **Radiofrequency ablation: Review of mechanism, indications, technique, and results.** *Chin J Radiol* 2001, **26**(3):119–134.
4. Sheu T, Chou C, Tsai S, Liang P: **Three-dimensional analysis for radio-frequency ablation of liver tumor with blood perfusion effect.** *Comput Methods Biomech Biomed Engin* 2005, **8**(4):229–240.
5. Frich L, Hol P, Roy S, Mala T, Edwin B, Clausen O, Gladhaug I: **Experimental hepatic radiofrequency ablation using wet electrodes: Electrode-to-vessel distance is a significant predictor for delayed portal vein thrombosis.** *Eur Radiol* 2006, **16**(9):1990–1999.
6. Wu F, Chen WZ, Bai J, Zou JZ, Wang ZL, Zhu H, Wang ZB: **Tumor vessel destruction resulting from high-intensity focused ultrasound in patients with solid malignancies.** *Ultrasound Med Biol* 2002, **28**(4):535–542.
7. Vaezy S, Zderic V: **Hemorrhage control using high intensity focused ultrasound.** *Int J Hyperthermia* 2007, **23**(2):203–211.

8. Zhang L, Zhu H, Jin C, Zhou K, Li K, Su H, Chen W, Bai J, Wang Z: **High-intensity focused ultrasound (HIFU): Effective and safe therapy for hepatocellular carcinoma adjacent to major hepatic veins.** *Eur Radiol* 2009, **19**(2):437–445.
9. Pennes H: **Analysis of tissue and arterial blood temperatures in the resting human forearm.** *J Appl Physiol* 1948, **1**(2):93–122.
10. Kolios M, Sherar M, Hunt J: **Large blood vessel cooling in heated tissues: A numerical study.** *Phys Med Biol* 1995, **40**(4):477–494.
11. Curra K, Mourad P, Khokhlova V, Cleveland R, Crum L: **Numerical simulations of heating patterns and tissue temperature response due to high-intensity focused ultrasound.** *IEEE Trans Ultrason Ferroelectr Freq Control* 2000, **47**(4):1077–1089.
12. Sheu TW, Solovchuk MA, Chen AW, Thiriet M: **On an acoustics-thermal-fluid coupling model for the prediction of temperature elevation in liver tumor.** *Int J Heat Mass Transf* 2011, **54**(17–18):4117–4126.
13. Solovchuk MA, Sheu TWH, Lin WL, Kuo I, Thiriet M: **Simulation study on acoustic streaming and convective cooling in blood vessels during a high-intensity focused ultrasound thermal ablation.** *Int J Heat Mass Transf* 2012, **55**(4):1261–1270.
14. Hamilton MF, Blackstock DT: *Nonlinear Acoustics*. Boston: Academic; 1998.
15. Hallaj I, Cleveland R: **FDTD simulation of finite-amplitude pressure and temperature fields for biomedical ultrasound.** *J Acoust Soc Am* 1999, **105**(5):L7–L12.
16. Pierce AD: *Acoustics: An Introduction to its Physical Principles and Applications*. Melville: Acoustical Society of America; 1991.
17. Sapareto S, Dewey W: **Thermal dose determination in cancer therapy.** *Int J Radiat Oncol Biol Phys* 1984, **10**(6):787–800.
18. Meaney P, Cahill M, Ter Haar G: **The intensity dependence of lesion position shift during focused ultrasound surgery.** *Ultrasound Med Biol* 2000, **26**(3):441–450.
19. Kamakura T, Matsuda K, Kumamoto Y, Breazeale M: **Acoustic streaming induced in focused Gaussian beams.** *J Acoust Soc Am* 1995, **97**(5 I):2740–2746.
20. Huang J, Holt R, Cleveland R, Roy R: **Experimental validation of a tractable numerical model for focused ultrasound heating in flow-through tissue phantoms.** *J Acoust Soc Am* 2004, **116**(4 I):2451–2458.
21. Sheu T, Hsieh L, Chen C: **Development of a three-point sixth-order Helmholtz scheme.** *J Comput Acoust* 2008, **16**(3):343–359.
22. Solovchuk MA, Sheu TWH, Thiriet M: **Simulation of nonlinear Westervelt equation for the investigation of acoustic streaming and nonlinear propagation effects.** *J Acoust Soc Am* 2013, **134**(5):3931-3942.
23. Duck F: *Physical Property of Tissues - A Comprehensive Reference Book*. London: Academic; 1990.
24. Solovchuk MA, Sheu TWH, Thiriet M, Lin WL: **On a computational study for investigating acoustic streaming and heating during focused ultrasound ablation of liver tumor.** *J Appl Thermal Eng* 2013, **56**(1–2):62–76.
25. Solovchuk MA, Sheu TWH, Thiriet M: **The effects of acoustic streaming on the temperature distribution during focused ultrasound therapy.** *AIP Conf Proc* 2012, **1433:**589.